Supplementary Materials for

A Low-Spin Manganese(II) Complex with an Emissive Charge-Transfer Excited State

Maxwell C. Rhames, Nora L. Burnett, Annemarie A. Lee, Colin B. Clark, William C. Tocco, Ahshabibi Ahmed, Alexander N. Ruhren, Claire Besson, Julien A. Panetier, John R. Swierk, Daniela M. Arias-Rotondo

Corresponding authors: Daniela M. Arias-Rotondo, dariasr@kzoo.edu; John R. Swierk, jswierk@binghamton.edu

The PDF file includes:

Materials and Methods

General. Reagents were purchased from commercial suppliers at the highest purity and were used without further purification. Air-sensitive samples were prepared using either standard Schlenk techniques or in a MBRAUN LABmaster 130 glovebox under a N_2 atmosphere. Nuclear magnetic resonance spectra were collected using a Bruker Avance III HD 400 MHz spectrometer at 400.13 MHz (^{1}H). All resonance spectra were reported in ppm and referenced to the residual solvent shifts [DMSO-d_6 (^{1}H δ = 2.050 ppm), acetonitrile-d_3 (^{1}H δ = 1.940 ppm)] as an internal standard. High performance liquid chromatography and mass spectrometry (HPLC-MS) was performed using a Waters Alliance e2690 with qDa mass detector and a UV-visible dual wavelength absorbance detector. HPLC analyses were performed on a 3.5 μm, 4.6 x 50 mm C18 Waters X-Bridge column at 40 °C using a 2-minute 100% acetonitrile isocratic method with a flowrate of 0.8 mL/min. Elemental analysis was performed by Midwest Microlab, Indianapolis, IN.

Syntheses

2,6-bis(3-phenylimidazolium-1-yl)pyridine dibromide, [H_2bim^{Ph}]Br_2.[1] A mixture of 2,6-dibromopyridine (2.4006 g, 10 mmol) and 1-phenylimidazole (2.691 mL, 21 mmol, 2.1 equiv.) was combined in a flask under N_2 and heated to 160 °C for 72 h, yielding a dark-tan solid adhered to the bottom of the flask which was then triturated with toluene (150 mL) under vigorous stirring overnight to remove any residual impurities. The product was then isolated via vacuum filtration and washed with toluene (4 x 10 mL), yielding an off-white solid. The product was dried further under high vacuum for 1 h. Yield: 1.836 g (3.496 mmol, 34%). ^{1}H NMR (400 MHz, DMSO) δ 10.88 (t, *J* = 1.6 Hz, 2H), 9.16 (t, *J* = 2.0 Hz, 2H), 8.75 (d, *J* = 8.1 Hz, 1H), 8.73 – 8.70 (m, 2H), 8.47 (d, *J* = 8.2 Hz, 2H), 8.02 – 7.65 (m, 10H).

2,6-bis(3-phenylimidazolium-1-yl)pyridine, [H_2bim^{Ph}]$(PF_6)_2$.[1] [H_2bim^{Ph}]Br_2 (0.9822 g, 1.9 mmol) was dissolved in a minimal amount of water under vigorous stirring. An aqueous solution of KPF_6 (4.4527 g, 20 mmol, 10 equiv) was added dropwise to the [H_2bim^{Ph}]Br_2 solution, leading to the immediate formation of a light-brown precipitate. The suspension was then allowed to stir overnight at room temperature before the solid was collected via vacuum filtration and washed with water (4 x 20 mL). Yield: 1.2251 g (1.869 mmol, 85%). ^{1}H NMR (400 MHz, CD_3CN) δ 9.85 (t, *J* = 1.7 Hz, 2H), 8.54 (t, *J* = 8.1 Hz, 1H), 8.45 (t, *J* = 2.0 Hz, 2H), 8.07 (d, *J* = 8.2 Hz, 2H), 8.05 (t, *J* = 1.7 Hz, 2H), 7.80 – 7.70 (m, 10H).

Manganese (II) triflate, $Mn(OTf)_2$. $MnCl_2 \bullet 4\ H_2O$ (0.4243 g, 2.1 mmol) was dissolved in MeOH (20 mL) and wrapped in aluminum foil to shield it from light. A solution of AgOTf (1.1328 g, 4.4 mmol, 2.1 equiv) in MeOH (10 mL) was slowly added into the solution of Mn(II) which resulted in the immediate formation of a white precipitate. Following the complete addition of AgOTf, the mixture was left to react while shielded from light for 1 h at room temperature. The reaction slurry was then filtered through celite, and the filtrate was concentrated under reduced pressure, yielding a brown viscous oil. A small aliquot of toluene (2 mL) was added to the oil before concentrating again under reduced pressure. The oil was then dried under high vacuum for several hours, yielding a fine white powder. Yield: 0.34 g (0.963 mmol, 45%).

[$Mn(bim^{Ph})_2$]$(PF_6)_2$.[2] [H_2bim^{Ph}]$(PF_6)_2$ (0.1573 g, 0.24 mmol, 2.4 equiv) was added to a flame-dried flask under N_2 and suspended in anhydrous THF (12 mL) before being cooled to 0°C in a NaCl/ice bath. LiHMDS (1 mL, 1 M, 10 equiv) in THF was added via syringe to the suspension of [H_2bim^{Ph}]$(PF_6)_2$ causing the immediate dissolution of the ligand and the generation of a yellow-

brown solution. The solution was left to react at 0 °C for 1 h before a degassed solution of $Mn(OTf)_2$ (0.0353 g, 0.1 mmol) in anhydrous THF (10 mL) was added slowly via cannula. The solution immediately turned black and was removed from the cold bath before being left to react under N_2 overnight. The crude reaction mixture was then concentrated under reduced pressure before adding acetonitrile (50 mL), yielding a deep-red solution and a fine black solid. The black solid was removed via vacuum filtration and the filtrate was concentrated under reduced pressure, generating a dark-red powder. Diffusion of diethyl ether into solutions of either acetonitrile or acetone yielded dark-red crystalline needles suitable for SC-XRD. Yield: 0.0169 g (0.0157 mmol, 16%). ESI-MS m/z [M^{2+}] Calculated: 390.61, found: 390.733. Anal. Calcd For $C_{46}H_{34}N_{10}MnP_2F_{12}$ C 51.55 H 3.20 N 13.07. Found C 51.67 H 3.54 N 13.15.

Physical Characterization

Single-crystal X-ray diffraction.

A dark red needle-shaped crystal (390 × 50 × 30 μm^3) was harvested from the diethylether/acetonitrile mother liquor and mounted on a 150 μm Mitegen mount. Diffraction data was collected at 296 K on a Rigaku XtaLAB Mini II equipped with a Mo Kα (λ = 0.71073 Å) X-ray source and a hybrid pixel detector, using 0.5° ω and φ scans. CrysAlisPro[3] was used for data reduction and analytical numeric absorption correction using a multifaceted crystal model.[4] The structure was solved using SHELXT[5] and refined in the *P21/n* space group with SHELXL[6] using Olex2[7] as the interface. All atoms except hydrogen atoms were refined anisotropically. Hydrogen atoms were placed in idealized positions and refined using a riding model. The PF_6^- counter ions show twofold disorder and were modeled as idealized octahedra using P-F and F-F distance restraints.

Table S1. Details on X-ray diffraction data collection and analysis

Crystal information	
CCDC Number	CCDC 2420773
Empirical formula	$MnC_{46}H_{34}F_{12}N_{10}P_2$
Crystal system	Monoclinic
Space group	$P2_1/n$ (#14)
a, *b*, *c* (Å)	16.3216(12), 13.6024(9), 20.9657(13)
β (°)	92.313(6)
Volume ()	4650.8(5)
Z	4
Data collection	
λ, Mo Kα (Å)	0.71073
Temperature (K)	296.8(10)
Theta range for data collection (°)	2.156-25.349
μ (mm^{-1})	0.448
Reflections collected	57139
Independent reflections	8532 [R(int) = 0.1091]
Refinement	
Method	Full matrix least square on F^2
Data/restraints/parameters	8532/1722/768
Goodness of fit	0.991
Residuals [$F^0>4\sigma(F^0)$]	R1 = 0.0710, wR2 = 0.1778
Largest diff. peak and hole (e.)	0.6 and -0.2

Optical absorption spectroscopy. Ground-state absorption spectroscopy and emission spectroscopy were performed using a Shimadzu UV-2600 spectrophotometer or Shimadzu RF-6000 Spectro Fluorometer, respectively. Spectra were collected at room-temperature in 10 mm quartz cuvettes with analyte solutions ranging in concentration from 10^{-6} to 10^{-5} M in spectroscopy-grade acetonitrile.

Electrochemistry. Electrochemical experiments were performed using a Bioanalytical Systems EC Epsilon potentiostat/galvanostat in a 0.1 M solution of tetrabutylammonium hexafluorophosphate (nBu$_4$N)(PF$_6$) in acetonitrile with a platinum working electrode, platinum counter-electrode, and silver pseudo-reference electrode. Cyclic voltammograms were collected under a N_2 atmosphere using a scan rate of 100 mV/s; all potentials were referenced to the Fc/Fc^+ redox-couple ($E_{1/2}$ = 485 mV under experimental conditions) as an internal standard.

Relative quantum yield of emission. Data were collected using the optical spectroscopic instruments described previously. A 4.56 x 10^{-6} M solution of degassed tris(2,2'-bipyridine)ruthenium(II) chloride was prepared via dilutions in acetonitrile and used as a relative standard for the excitation peak at 480 nm (Φ = 0.095).[8] A 2.90 x 10^{-6} M cresyl violet solution was prepared via dilutions in acetonitrile and used as a relative standard for the excitation peak at 600 nm (Φ = 0.054).[8] The solutions were prepared in the same solvent, measured with the same

instrumental parameters, and had similar absorbance readings to $[Mn(bim^{Ph})_2](PF_6)_2$. Relative quantum yields of emission were calculated according to the method described by Arias-Rotondo and McCusker.[9]

Time-resolved Transient Emission Spectroscopy.[10] Fluorescence decay lifetime data were collected using a time-correlated single photon counting (TCSPC) instrument with a CW passively mode-locked, diode-pumped Nd:YVO_4 laser. The output of the laser pumps a cavity-dumped dye laser (Coherent 702-2) operating between 430 and 850 nm with 5 ps pulses. A 40× reflecting microscope objective is used to detect emission before it is separated into polarization components parallel (0^o) and perpendicular (90^o) to the vertically polarized excitation pulse with a polarizing cube beam splitter. These signals are detected simultaneously using microchannel plate photomultiplier tubes (MCP-PMT, Hamamatsu R3809U-50) with a subtractive double monochromator (Spectral Products CM-112) for selective emission wavelength detection. The parallel and perpendicular transients are resolved independently yielding an instrumental response function of roughly 30 ps. Data are collected using multichannel analyzers (MCAs) and data acquisition, detector bias, and collection wavelength are all controlled using an in-house written LabVIEW (National Instruments) program.

Computational Details. Density functional theory (DFT) calculations were carried out with Gaussian 16 (Revision A.03).[11] Geometry optimizations were performed at the unrestricted B3LYP-D3(BJ)[12,13] level of theory in acetonitrile (ε = 35.688) through the solvation model based on density (SMD) approach.[14] The Def2-TZVP basis set was used on Mn, while the Def2-SVP basis set was employed on all other atoms (denoted BS1).[15,16] Additional single-point calculations were run in solution using the Def2-TZVPP basis set for all atoms (denoted BS2).[15,16] Exchange correlation integrals were evaluated with a quadrature grid of 99 radial shells and 590 angular points per shell. Stability analyses were performed in addition to analytical frequency calculations on all stationary points to ensure that geometries correspond to local minima (all positive eigenvalues). All computed free energies include the zero-point vibrational energy corrections, thermal corrections, and entropies calculated by standard statistical thermodynamic methods at 298.15 K and 1 atm. The computed Gibbs free energies were corrected by implementing Grimme's quasi-harmonic approach to entropic contributions and Head-Gordon's quasi-harmonic approach to enthalpy.[16,17] Time-dependent DFT (TD-DFT) calculations were done using the same methodology. We note that the B3LYP functional has been shown to provide good agreement with experimental UV-Vis spectra for copper transition-metal complexes featuring NHC ligands.[18]

Evans method for Solution-phase Magnetic Susceptibility Measurements. A 2% v/v solution of acetonitrile in acetonitrile-d_3 was prepared and an aliquot was sealed within a capillary tube. A ~5 mM analyte solution was then prepared by dissolving 3-5 mg of solid in roughly 600 µL of the 2% acetonitrile solution before being transferred to an NMR tube. The sealed capillary tube containing the 2% acetonitrile reference was then added to the same tube prior to the NMR tube being sealed tightly with a cap. 400 MHz ^{1}H NMR spectroscopy was then employed to determine the difference in frequency (Δν) in Hz of the acetonitrile reference signals for the inner and outer tubes. This value was then used along with the frequency of the spectrometer (ν) in Hz and the concentration of the paramagnetic species (c) in g cm^{-3} to calculate the mass susceptibility (χ). A correction was also applied for accounting for the specific susceptibility of the pure deuterated solvent ($\chi_o = -0.534 \times 10^{-6}$ cm^3 g^{-1})[19,20] (Equation 1) and the change in density between the solvent ($d_0 = 0.842$ g.cm^{-3}) and the solution ($d_s = 0.845 \pm 0.002$ g.cm^{-3}).[21,22]

$$\chi = \frac{3\,\Delta\nu}{4\pi\nu c} + \chi_o + \chi_o \frac{d_0 - d_s}{c} \qquad (1)$$

The molar susceptibility (χ_m) was then calculated by accounting for the molar mass of the analyte species. The diamagnetic molar susceptibility χ_{dia} = -0.535×10^{-3} cm^3.mol^{-1} was estimated using Pascal's constants[23] and subtracted from the molar susceptibility to yield the paramagnetic susceptibility

$$\chi_p = \chi_m - \chi_{dia} \quad (2)$$

The effective magnetic moment (μ_{eff}) at T = 300 K was then calculated by

$$\mu_{eff} = \sqrt{8\chi_p T} \quad (3)$$

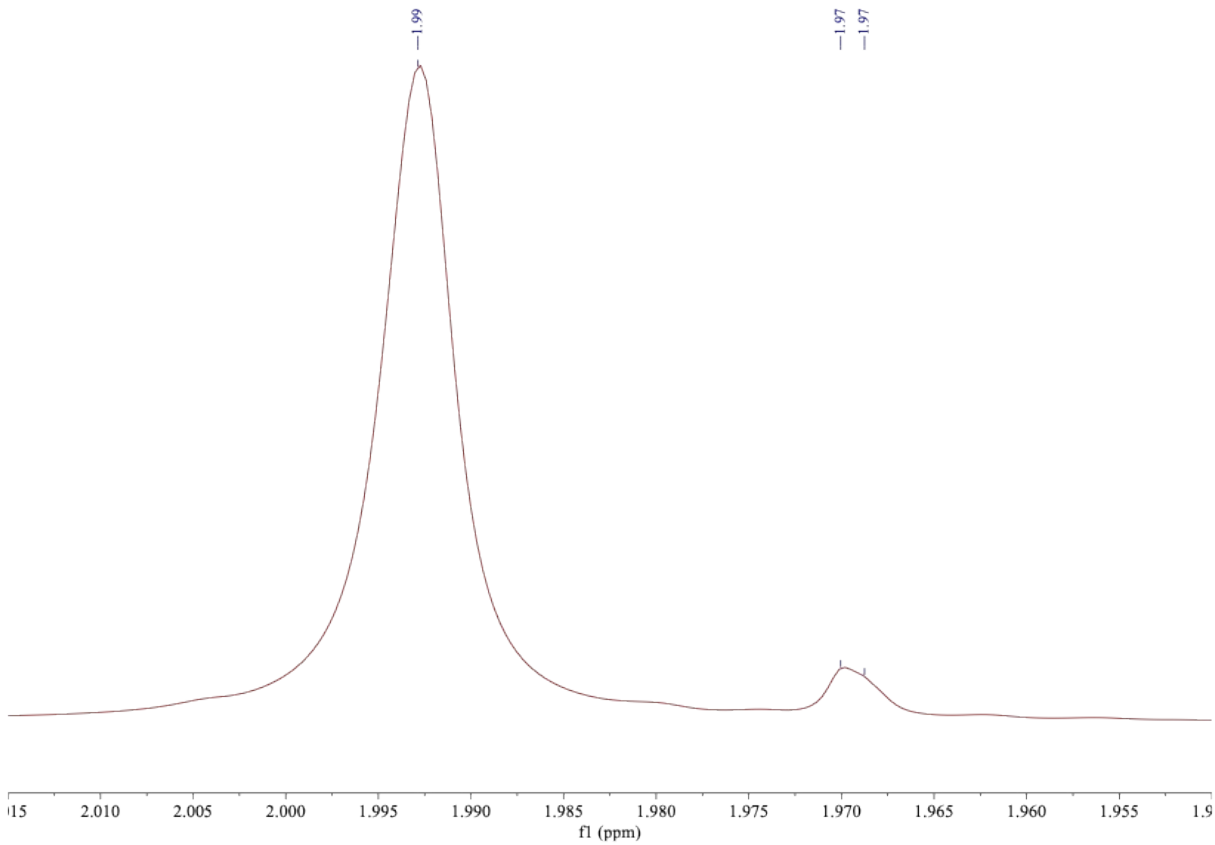

Figure S1. 400 MHz ^{1}H NMR spectrum via the Evans method for magnetic susceptibility measurements. The large peak at 1.99 ppm is the shifted acetonitrile signal due to the presence of the analyte, [Mn(bim^{Ph})$_2$](PF$_6$)$_2$. The weaker signal at 1.97 is the reference acetonitrile solution.

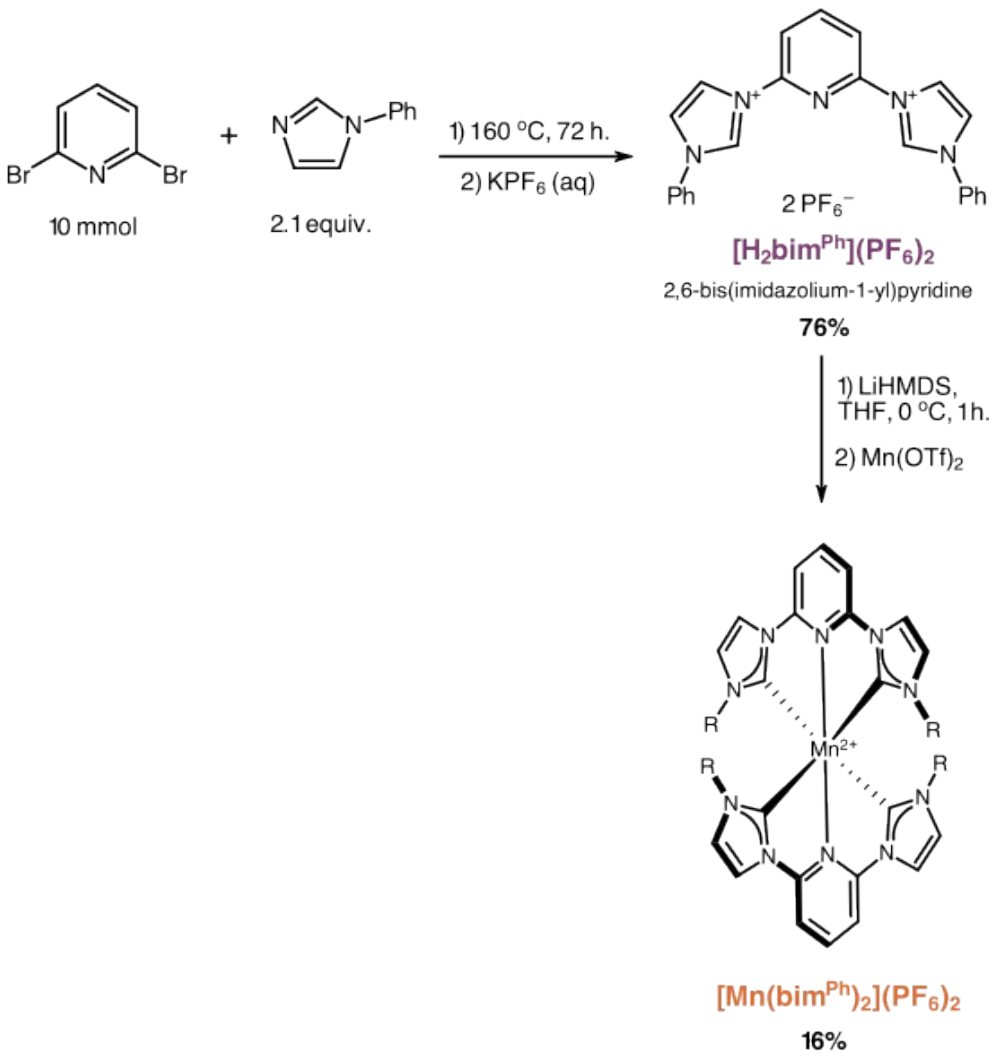

Fig. S2. Synthetic route to prepare $[Mn(bim^{Ph})_2](PF_6)_2$.

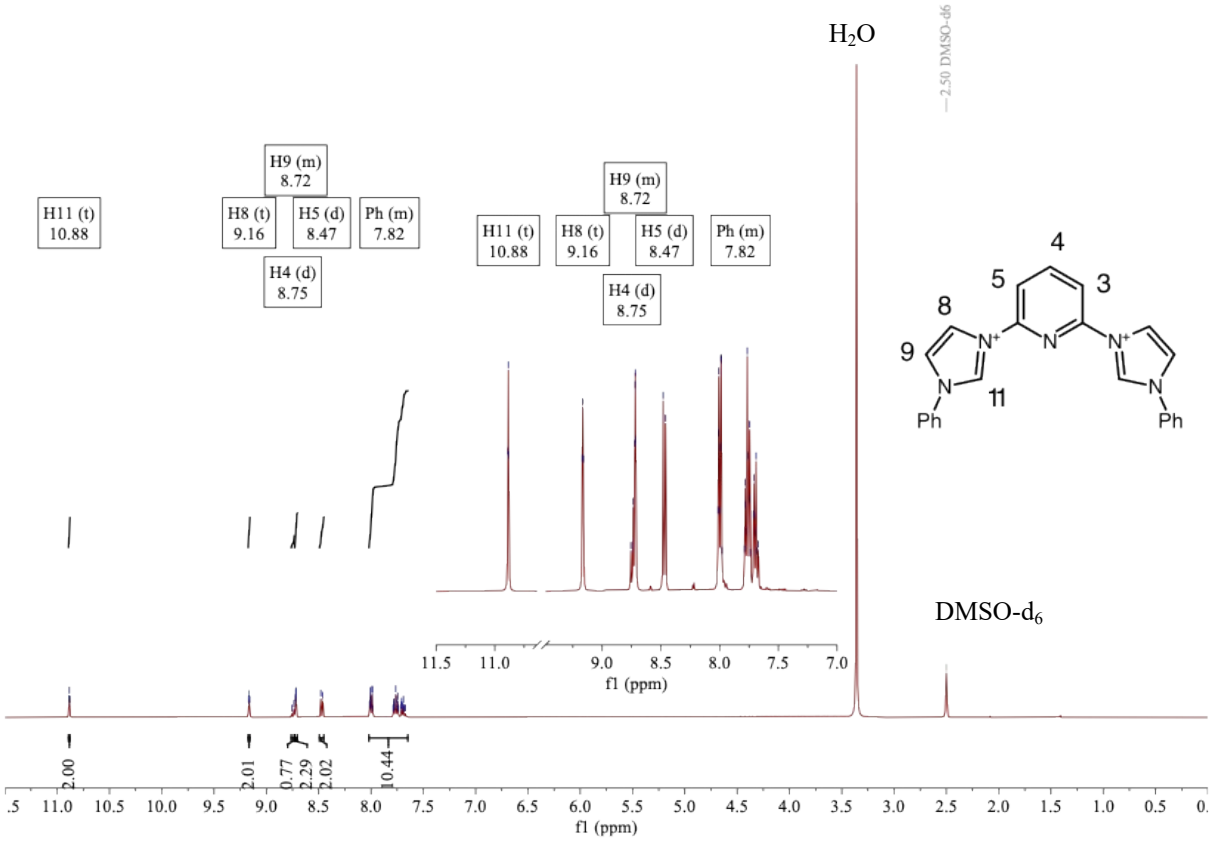

Fig. S3. 400 MHz ^{1}H NMR spectrum of $[H_2bim^{Ph}]Br_2$ in DMSO-d_6.

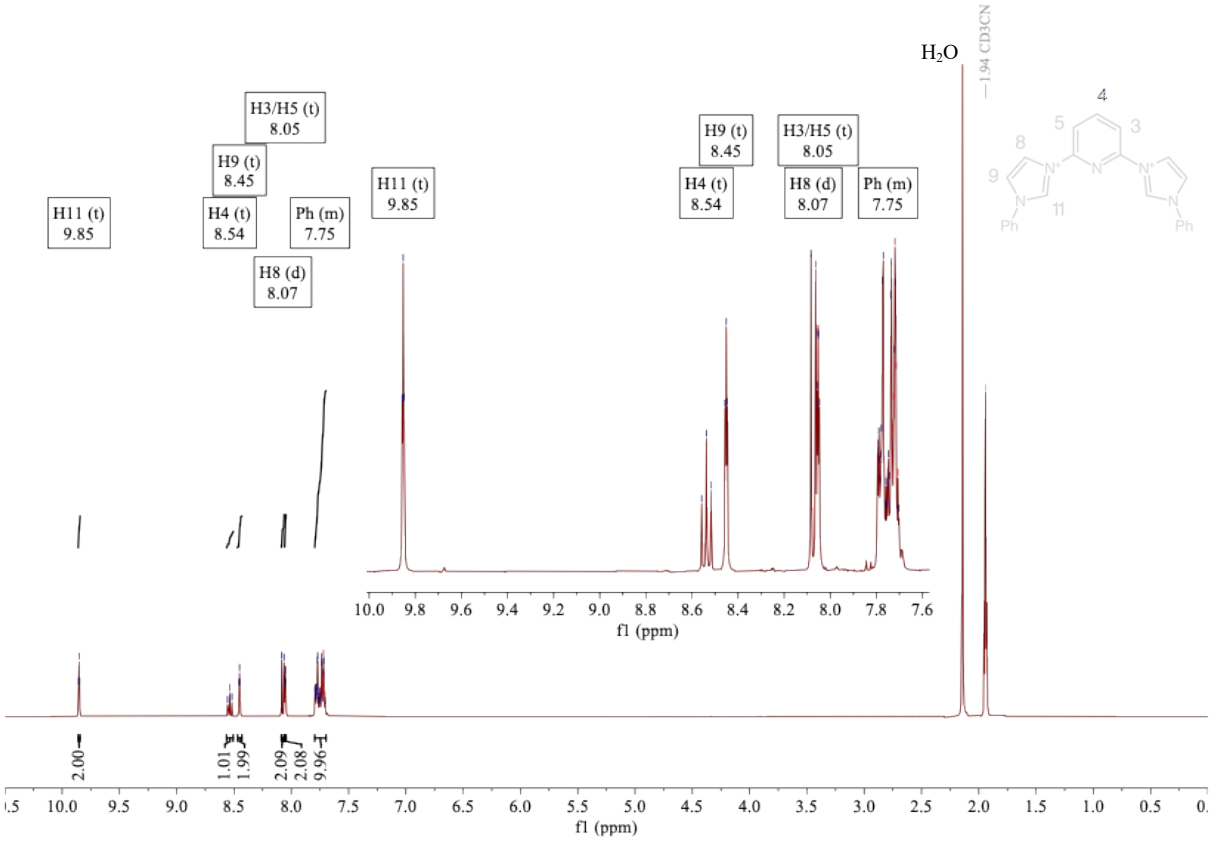

Fig. S4. 400 MHz ^{1}H NMR spectrum of $[H_2bim^{Ph}](PF_6)_2$ in in MeCN-d_3.

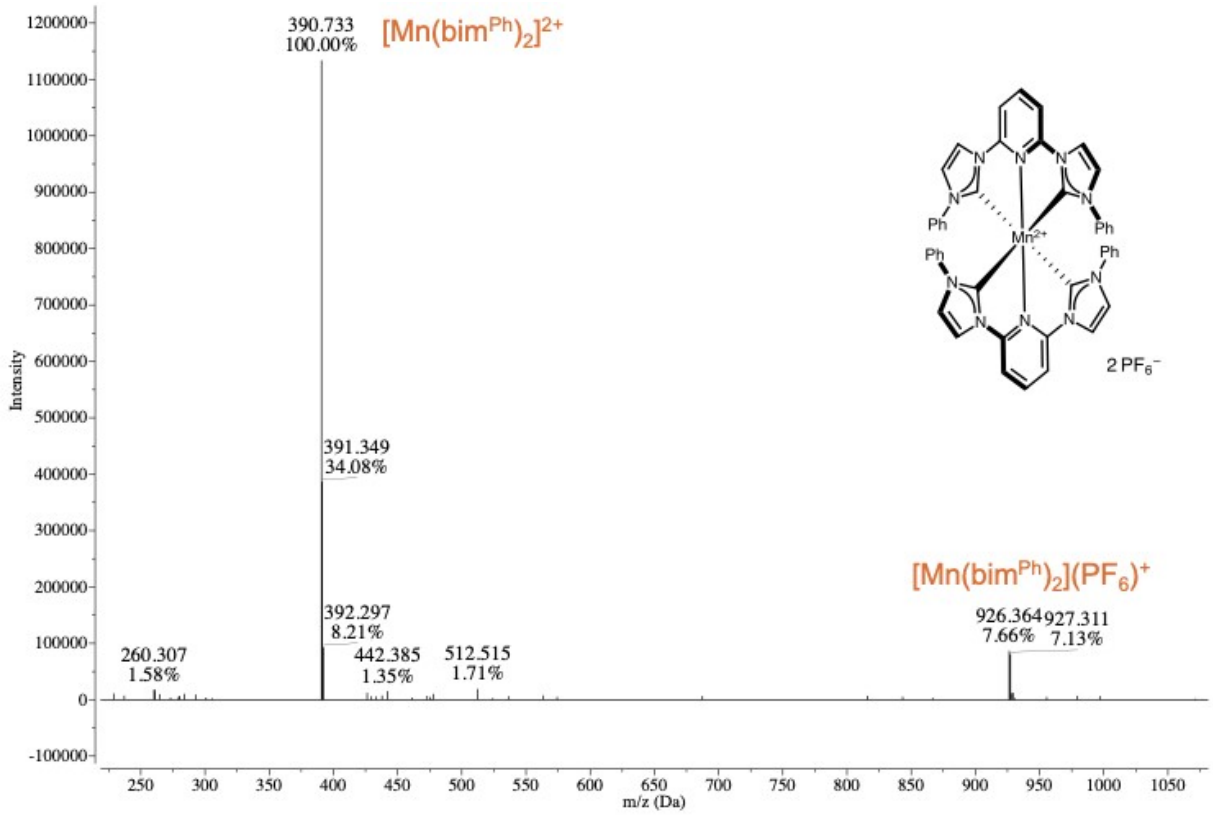

Fig. S5. Mass spectrum of $[Mn(bim^{Ph})_2](PF_6)_2$. Intensities are given with respect to the most intense peak.

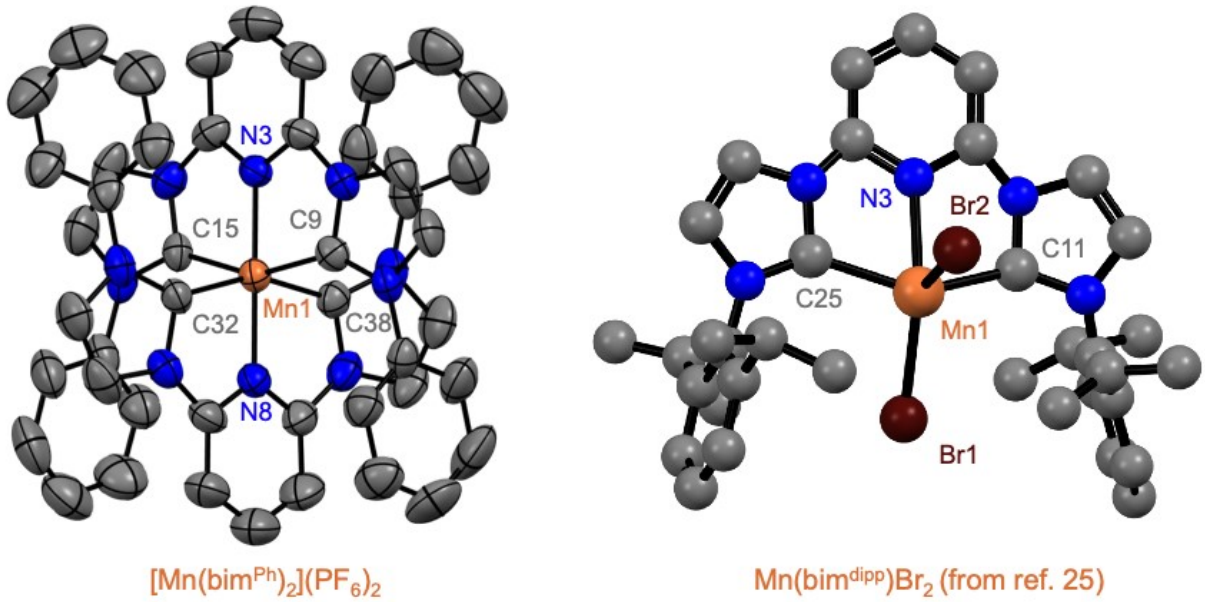

Fig. S6. Crystal structural comparison of $[Mn(bim^{Ph})_2](PF_6)_2$ (left) and $Mn(bim^{dipp})Br_2$ (right) with selected atom labels. Thermal ellipsoids are shown at 50% probability for $[Mn(bim^{Ph})_2](PF_6)_2$. Hydrogen atoms and PF_6^- ions are omitted for clarity. Color code: C (gray), N (blue), Mn (orange), Br (brown).

Table S2. Comparison of the selected bond lengths of $[Mn(bim^{Ph})_2](PF_6)_2$ and $Mn(bim^{Dipp})Br_2$.

$[Mn(bim^{Ph})_2](PF_6)_2$[a]		**$Mn(bim^{Dipp})Br_2$[b]**	
Selected Bonds	Selected Bond Lengths (Å)	Selected Bonds	Selected Bond Lengths (Å)
Mn-C9	1.987(5)	Mn(1A)-C(13A)	2.206(2)
Mn-C15	1.990(5)	Mn(1A)-C(21A)	2.210(2)
Mn-C32	1.997(5)	Mn(1A)-N(3A)	2.2574(16)
Mn-C38	1.982(5)	Mn(1A)-Br(1A)	2.5458(7)
Mn-N3	1.957(4)	Mn(1A)-Br(2A)	2.5708(7)
Mn-N8	1.958(4)		

[a]This work. [b]Pugh et al.[24]

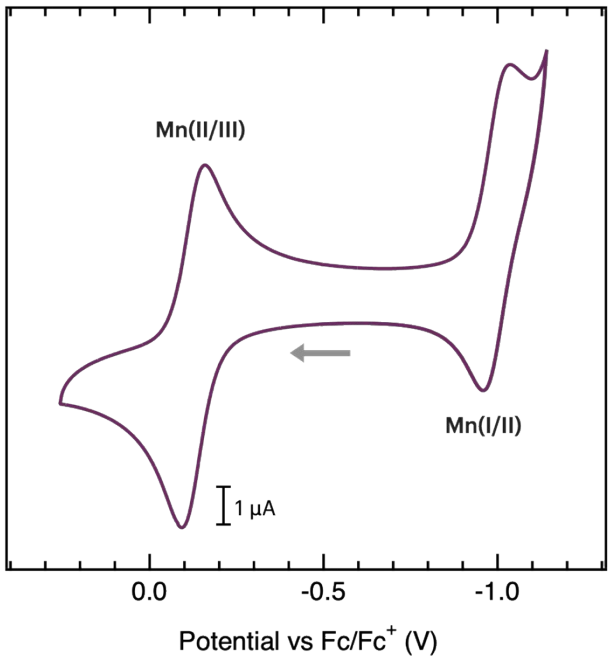

Fig. S7. Cyclic voltammogram of $[Mn(bim^{Ph})_2](PF_6)_2$ in acetonitrile with 0.1 M $(n\text{Bu})_4(PF_6)_2$ as a supporting electrolyte. Arrow indicates the potential sweep direction.

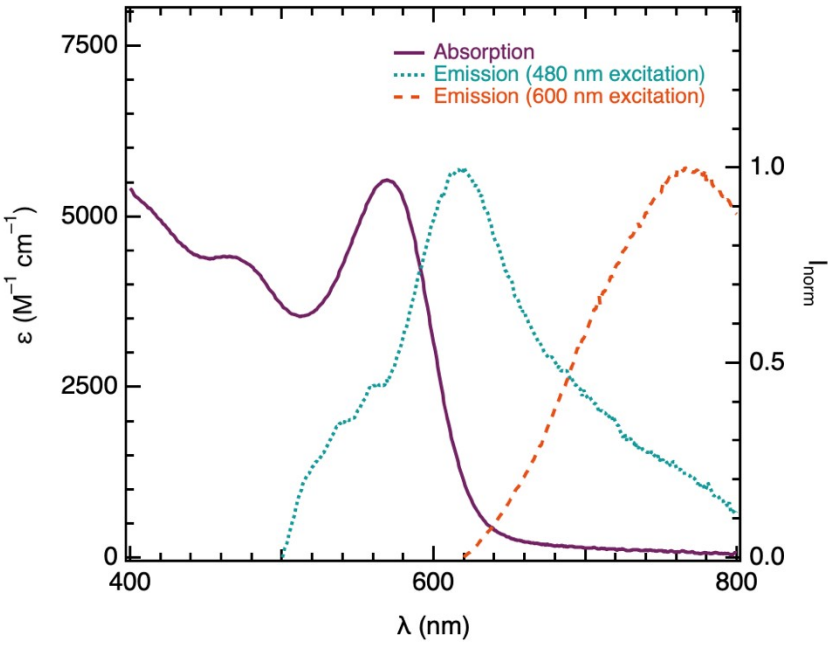

Fig. S8. Steady-state emission spectra of $[Mn(bim^{Ph})_2](PF_6)_2$ collected in acetonitrile, under air. The solid purple line is the electronic absorption spectrum of the complex. Emission at λ_{exc} = 480 nm is shown in the dotted green trace. Emission at λ_{exc} = 600 nm is shown in the dashed orange trace.

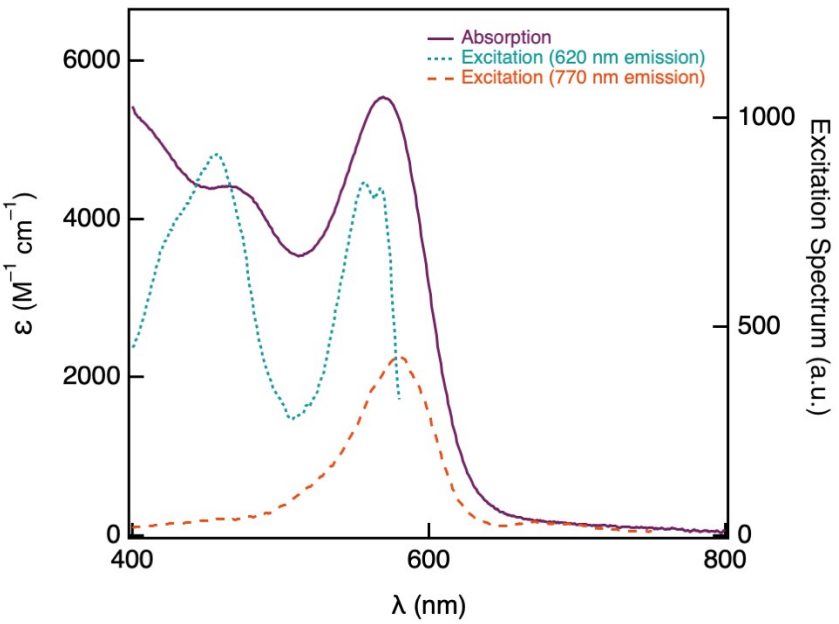

Fig. S9. Comparison of the excitation and absorption spectra for $[Mn(bim^{Ph})_2](PF_6)_2$ in acetonitrile. The solid purple line is the electronic absorption spectrum of the complex. Excitation for λ_{em} = 620 nm is shown in the dotted green trace. Excitation for λ_{em} = 770 nm is shown in the dashed orange trace.

As shown in Fig. S8, Excitation at 480 nm results in an emission band with a maximum at approximately 620 nm (QY = 1.9 x10^{-3}). Conversely, excitation into the band at 600 nm gives rise to a broad emission band that peaks around 770 nm (QY = 5.7 x10^{-4}). The excitation spectrum for the 620 nm emission band matches the UV-vis spectrum of $[Mn(bim^{Ph})_2](PF_6)_2$ reasonably well (Figure S9), showing that light absorption between 400 and 500 nm or between 530 and 580 nm results in emission at 620 nm. Conversely, the excitation spectrum for the 770 nm emission band shows that this excited state is only accessible through excitation at redder wavelengths (530 through 610 nm). These two emission bands generated via excitation at different wavelengths are consistent with two excited states that can be accessed independently.

Because this is an uncommon occurrence for a transition-metal complex, we investigated whether the second emission was an artifact or an impurity. The protonated ligand precursor, $[H_2bim^{Ph}](PF_6)_2$, does not emit in the visible range (Fig. S10), and all emission experiments were done under air, so it is unlikely that any bands correspond to the deprotonated ligand (bimPh), as this di-carbene species is highly reactive in the presence of water or air. Together, these strongly suggest that both emission bands correspond to Mn-containing species. Emission spectra were collected multiple times from separate samples, all of which were recrystallized more than once. A representative HLPC-MS trace (Fig. S5) reveals the presence of very small impurity peaks (all are <2%). If either of the emission bands seen in Fig. S8 was due to an impurity, then the quantum yield of emission of such a compound should be much higher 10%, based on the relative intensities of the bands and the concentration of the presumed impurity (and its necessarily low light-harvesting ability); such a highly emissive Mn-containing impurity is unlikely. Another possibility would be the presence of an S = 5/2 compound, the product of spin crossover. If this was the case,

the intensity of the emission should track the concentration of the S = 5/2 species as temperature changes. Variable-temperature emission data show this is not the case, as the ratio of the two bands remains constant over a wide temperature range (Table S3). The combination of the lack of emission from the protonated ligand precursor, the agreement between the excitation and absorption spectra, as well as the quantum yield of emission of both bands suggests that $[Mn(bim^{Ph})_2]^{2+}$ can access two emissive excited states. Transient absorption data for this complex will shed light on the evolution of both these states. Work along these lines is underway.

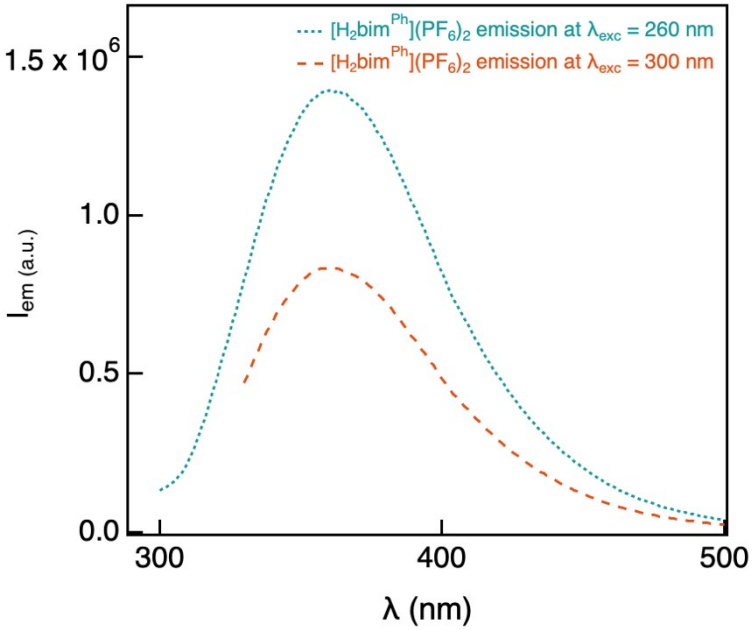

Fig. S10. Steady-state emission spectra of $[H_2bim^{Ph}](PF_6)_2$ collected in acetonitrile. Emission at λ_{exc} = 260 nm is shown in the dashed blue trace. Emission at λ_{exc} = 300 nm is shown in the dashed orange trace.

Table S3. Ratio of the intensities of the emission peaks at 770 nm and 620 nm at several temperatures.

Temperature (ºC)	$I_{770\ nm}/I_{620\ nm}$
0	5.0
10	5.3
20	5.3
30	5.5
40	5.3
50	5.4
60	5.7

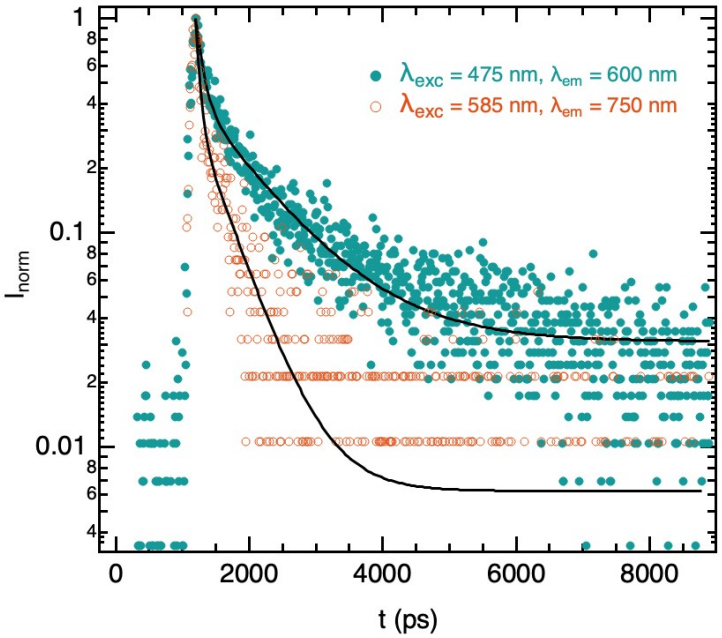

Fig. S11. Time-resolved emission spectra of $[Mn(bim^{Ph})_2](PF_6)_2$ collected in acetonitrile. The excited state decay trace for λ_{exc} = 475 nm and λ_{em} = 600 nm is represented in solid green circles (τ_1 = 106 ± 6 ps and τ_2 = 1.0 ± 0.3 ns). The decay trace for λ_{exc} = 585 nm and λ_{em} = 750 nm is shown in open orange circles (τ_1 < 60 ps and τ_2 = 480 ± 20 ps). Both traces are fitted with a double exponential (black line).

Time-resolved emission spectroscopy data were fitted to a double exponential, according to equation 4.

$$y = y_0 + A_1 exp\left\{\frac{-(x - x_0)}{\tau_1}\right\} + A_2 exp\left\{\frac{-(x - x_0)}{\tau_2}\right\} \quad (4)$$

The fitting parameters for the traces shown in Figures 4 and S11 are collected in Table S4.

Table S4. Parameters used to fit the traces in Figures 4 and S11 to a double exponential decay. The only constant value is x_0.

Data set	y_0	A_1	x_0	τ_1	A_2	τ_2
λ_{exc} = 475 nm λ_{em} = 600 nm	0.031 ± 0.001	0.58 ± 0.02	1200 ps	106 ± 6 ps	0.38 ± 0.01	1000 ± 30 ps
λ_{exc} = 585 nm λ_{em} = 750 nm	0.0062 ± 0.0009	0.68 ± 0.02	1200 ps	57 ± 3 ps	0.32 ± 0.02	480 ± 20 ps

Table S5. Calculated relative energies for $[Mn(bim^{Ph})_2]^{2+}$ at the B3LYP-D3(BJ)/BS1(SMD) level of theory. The Mulliken spin population is given for manganese, ρ_{Mn}. [a]As shown in Table S7, the Mn–C and Mn–N bonds are significantly elongated.

Multiplicity	$<S^2>$	ρ_{Mn}	ΔE	ΔZPE	ΔG
S = 1/2	0.78	1.22	0.0	0.0	0.0
S =3/2	3.90	3.23	9.1	7.7	5.6
S = 5/2[a]	8.76	4.80	-1.2	-2.5	-5.7

Table S6 Calculated relative energies for $[Mn(bim^{Ph})_2]^{2+}$ at the B3LYP-D3(BJ)/BS2(SMD) level of theory. The Mulliken spin population is given for manganese, ρ_{Mn}. [a]As shown in Table S7, the Mn–C and Mn–N bonds are significantly elongated.

Multiplicity	$<S^2>$	ρ_{Mn}	ΔE	ΔZPE	ΔG
S = 1/2	0.78	1.27	0.0	0.0	0.0
S =3/2	3.89	3.21	8.5	7.1	5.0

S = 5/2[a]	8.76	4.85	-3.8	-5.1	-8.3

Table S7. Comparison of the experimental and computed bond distances for $[Mn(bim^{Ph})_2]^{2+}$. Both doublet (S = 1/2) and sextet (S = 5/2) computed bond distances are reported. Distances are in Å.

	Experimental	**Calculated (S = 1/2)**	**Calculated (S = 5/2)**
Mn-C9	1.987(5)	2.01	2.31
Mn-C15	1.990(5)	2.01	2.30
Mn-C32	1.997(5)	2.01	2.30
Mn-C38	1.982(5)	2.01	2.32
Mn-N3	1.957(4)	1.99	2.48
Mn-N8	1.958(4)	1.99	2.48

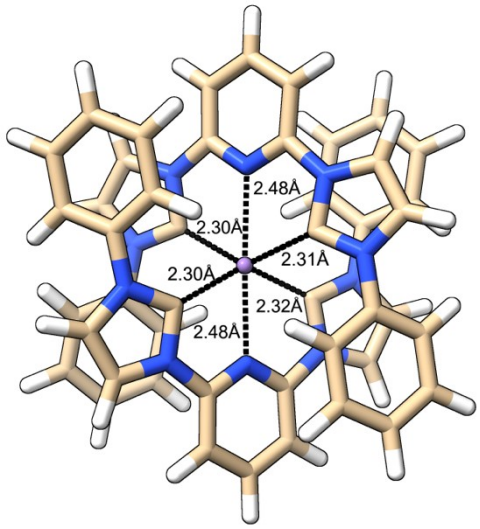

Fig. S12. Computed geometry of the sextet spin state showing the elongation of the Mn-N bond distances to 2.48 Å.

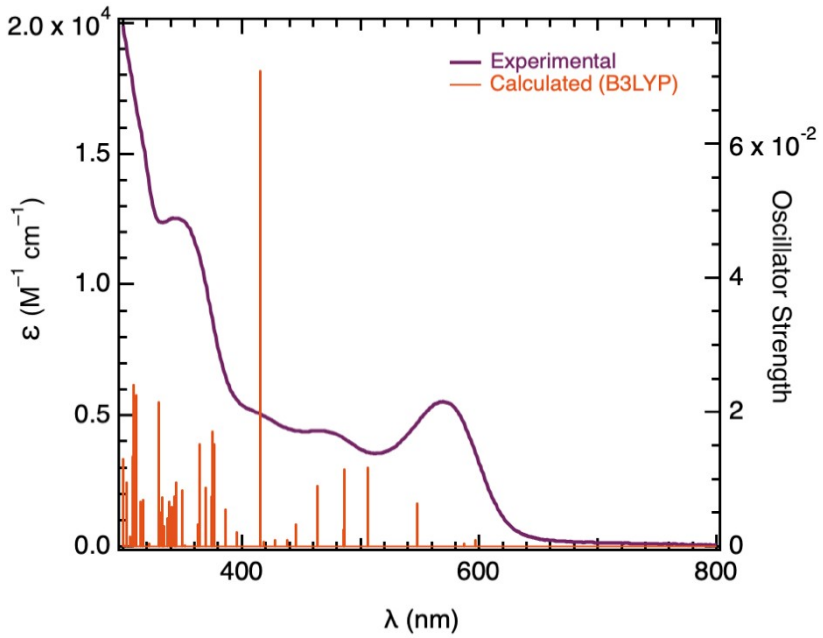

Fig. S13. Experimental electronic absorption spectrum (purple line) and computed oscillator strength (orange) for $[Mn(bim^{Ph})_2]^{2+}$ (S = ½) using the B3LYP-B3(BJ) functional in acetonitrile.

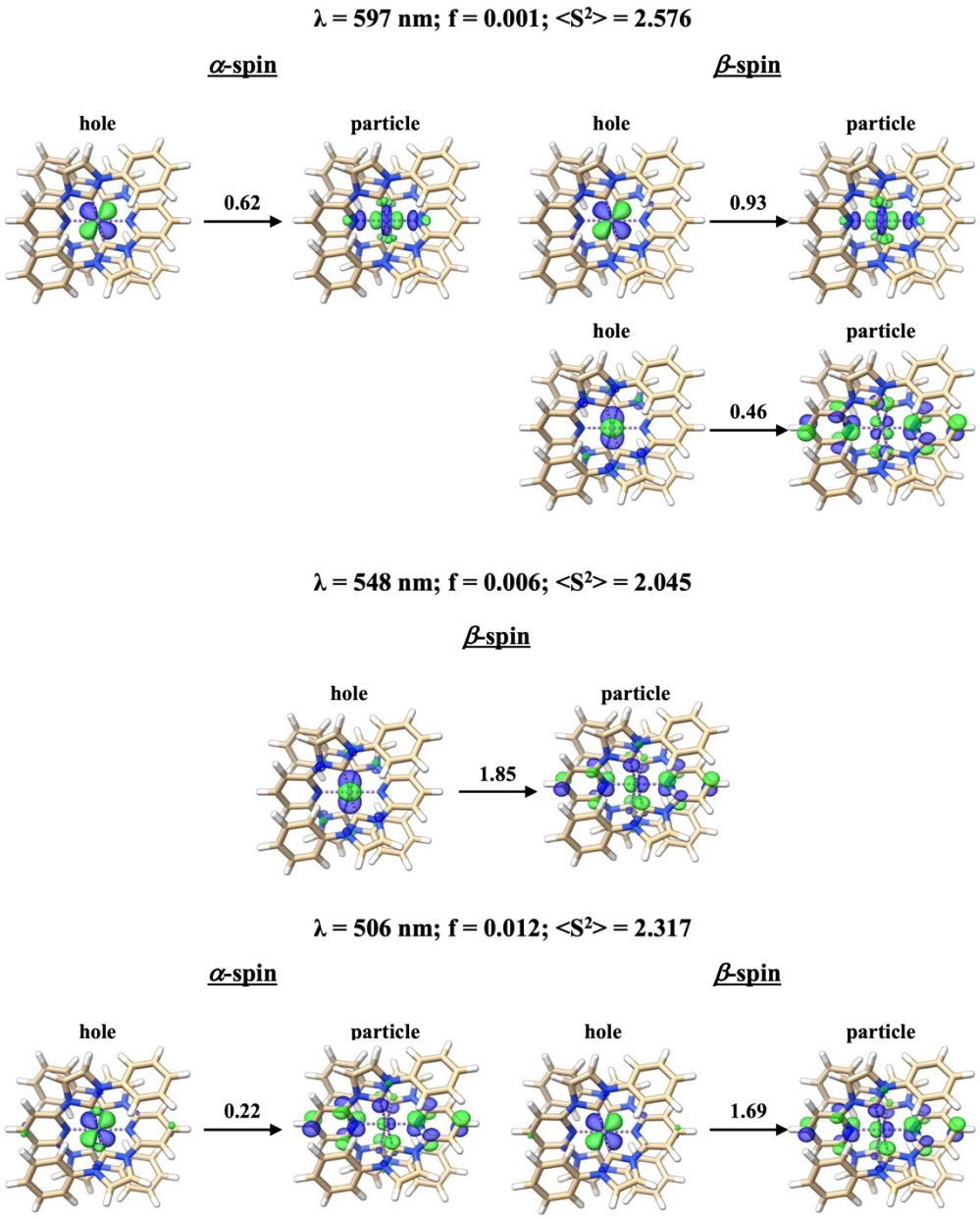

Fig. S14. Isosurface plots of the dominant natural transition orbital pairs for the computed excited states in the region of 500 to 600 nm.

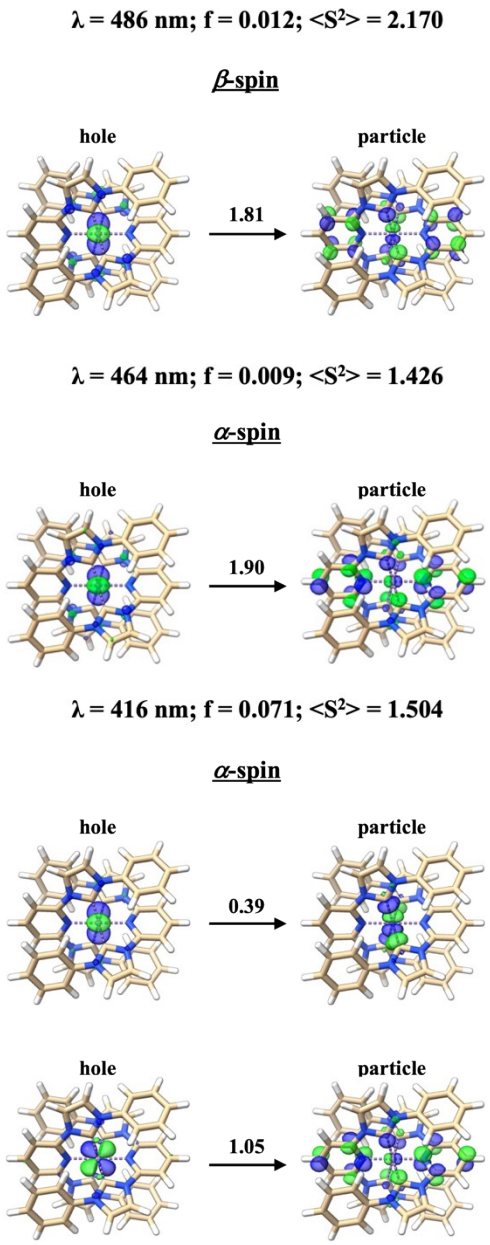

Fig. S15. Isosurface plots of the dominant natural transition orbital pairs for the computed excited states in the region of 400 to 500 nm.

We note that most oscillator strengths for the transitions described above are relatively weak (e.g., less than 10^{-2}). One possible explanation is that many of these transitions are spin contaminated. In fact, the $\langle S^2 \rangle$ value significantly diverges from the expected 0.75 for spin-allowed doublet-to-doublet transitions. Although further computational and experimental studies are currently underway, our current TD-DFT calculations indicate that at λ_{calc} = 597 nm, a higher-spin-state species may participate in the transition, which aligns with an $\langle S^2 \rangle$ value of 2.6 and accounts for the weak oscillator strength (f = 0.001, see Figure S14). Conversely, the lower $\langle S^2 \rangle$ value of 1.5

at λ_{calc} = 416 nm suggests that this transition predominantly involves a doublet-to-doublet transition, resulting in a higher oscillator strength (f = 0.071, see Figure S15).

Cartesian Coordinates and Computed Energies (a.u.) for $[Mn(bim^{Ph})_2]^{2+}$ at the B3LYP-D3(BJ)/BS2(SMD) level of theory.

$[Mn(bim^{Ph})_2]^{2+}$ (S = 1/2)

Energy = -3470.36815590
Enthalpy 0K = -3469.653578
Enthalpy 298K = -3469.609880
Free Energy 298K = -3469.729320
Nimag = 0 (23.6349 cm^{-1})

Mn	0.00002	-0.00001	-0.00002
N	0.15739	2.56372	1.87736
N	-1.77541	1.74719	1.40831
N	-1.99236	-0.00003	0.00015
N	-1.77560	-1.74724	-1.40804
N	0.15715	-2.56371	-1.87740
N	-0.15705	-2.56350	1.87761
N	1.77569	-1.74703	1.40819
N	1.99239	0.00005	-0.00019
N	1.77536	1.74713	-1.40851
N	-0.15749	2.56356	-1.87755
C	1.56947	2.77576	1.94436
C	2.38151	1.83963	2.58984
H	1.93062	0.95904	3.04879
C	3.76079	2.04925	2.63562
H	4.40040	1.31782	3.13356
C	4.32036	3.18704	2.04522
H	5.40057	3.34562	2.08149
C	3.49850	4.11796	1.40232
H	3.93296	5.00296	0.93193
C	2.11761	3.91380	1.34617
H	1.46474	4.62095	0.83148
C	-0.80084	3.45119	2.38776
H	-0.51570	4.35110	2.92550
C	-2.02058	2.93630	2.09428
H	-3.02337	3.29770	2.30187
C	-0.42169	1.50568	1.26046
C	-2.65935	0.90333	0.73367
C	-4.04944	0.94706	0.76617
H	-4.57269	1.68936	1.36697
C	-4.73653	-0.00008	0.00041
H	-5.82798	-0.00011	0.00052

C -4.04955 -0.94720 -0.76547
H -4.57288 -1.68953 -1.36616
C -2.65945 -0.90342 -0.73324
C -0.42186 -1.50570 -1.26039
C -2.02085 -2.93634 -2.09400
H -3.02366 -3.29777 -2.30145
C -0.80114 -3.45118 -2.38768
H -0.51605 -4.35107 -2.92549
C 2.38115 -1.83961 -2.59023
H 1.93018 -0.95904 -3.04915
C 3.76043 -2.04921 -2.63622
H 4.39995 -1.31778 -3.13428
C 4.32010 -3.18697 -2.04586
H 5.40031 -3.34554 -2.08229
C 3.49835 -4.11788 -1.40280
H 3.93290 -5.00286 -0.93244
C 2.11746 -3.91374 -1.34645
H 1.46468 -4.62087 -0.83163
C 1.56922 -2.77572 -1.94460
C -1.56912 -2.77556 1.94472
C -2.38114 -1.83933 2.59007
H -1.93024 -0.95866 3.04888
C -3.76042 -2.04892 2.63589
H -4.40002 -1.31740 3.13372
C -4.32001 -3.18679 2.04566
H -5.40023 -3.34535 2.08196
C -3.49817 -4.11782 1.40288
H -3.93265 -5.00287 0.93261
C -2.11727 -3.91367 1.34668
H -1.46442 -4.62088 0.83206
C 0.80126 -3.45087 2.38805
H 0.51619 -4.35070 2.92596
C 2.02096 -2.93603 2.09431
H 3.02378 -3.29740 2.30182
C 0.42195 -1.50554 1.26050
C 2.65952 -0.90325 0.73329
C 4.04961 -0.94697 0.76551
H 4.57298 -1.68922 1.36628
C 4.73656 0.00009 -0.00047
H 5.82800 0.00010 -0.00059
C 4.04943 0.94714 -0.76631
H 4.57265 1.68939 -1.36720
C 2.65934 0.90337 -0.73379
C 0.42165 1.50558 -1.26061
C 2.02046 2.93619 -2.09458
H 3.02323 3.29762 -2.30222

C 0.80069 3.45100 -2.38808
H 0.51549 4.35086 -2.92588
C -2.11772 3.91361 -1.34634
H -1.46483 4.62088 -0.83183
C -3.49864 4.11766 -1.40231
H -3.93310 5.00269 -0.93198
C -4.32052 3.18657 -2.04494
H -5.40076 3.34506 -2.08106
C -3.76095 2.04873 -2.63525
H -4.40059 1.31717 -3.13297
C -2.38165 1.83924 -2.58966
H -1.93076 0.95859 -3.04852
C -1.56958 2.77552 -1.94445

$[Mn(bim^{Ph})_2]^{2+}$ (S = 3/2)

Energy = -3470.35372876
Enthalpy 0K = -3469.641375
Enthalpy 298K = -3469.596473
Free Energy 298K = -3469.721364
Nimag = 0 (17.9130 cm^{-1})

Mn 0.00001 -0.00168 -0.00002
N -0.10661 2.58019 1.89554
N -2.00705 1.74224 1.34077
N -2.24245 -0.03493 -0.02570
N -1.92948 -1.79226 -1.40321
N 0.00109 -2.58201 -1.91870
N -0.00091 -2.58222 1.91835
N 1.92961 -1.79232 1.40291
N 2.24247 -0.03483 0.02558
N 2.00694 1.74254 -1.34061
N 0.10644 2.58042 -1.89524
C 1.30149 2.80151 1.99297
C 2.11504 1.83067 2.58330
H 1.66571 0.92351 2.98819
C 3.49397 2.03855 2.64083
H 4.13439 1.28096 3.09662
C 4.05258 3.20713 2.11285
H 5.13299 3.36288 2.15420
C 3.22882 4.17370 1.52725
H 3.66215 5.08383 1.10645
C 1.84772 3.97346 1.46234
H 1.19566 4.70901 0.98812
C -1.09018 3.46333 2.35364
H -0.83966 4.37221 2.89363

C -2.28990 2.93300 2.00576
H -3.30355 3.29002 2.16199
C -0.64579 1.51238 1.26168
C -2.89649 0.87704 0.67218
C -4.29106 0.91791 0.68597
H -4.84053 1.66025 1.26334
C -4.94942 -0.04907 -0.08480
H -6.04105 -0.05568 -0.10760
C -4.24772 -1.00678 -0.82893
H -4.76375 -1.75228 -1.43264
C -2.85576 -0.94899 -0.75690
C -0.57622 -1.53034 -1.29271
C -2.16988 -2.98544 -2.07992
H -3.17137 -3.36433 -2.26094
C -0.95038 -3.48610 -2.40274
H -0.66550 -4.38652 -2.93988
C 2.21334 -1.81118 -2.61600
H 1.74723 -0.93725 -3.07228
C 3.59806 -1.98549 -2.64317
H 4.22641 -1.23608 -3.12846
C 4.17739 -3.11016 -2.04697
H 5.26194 -3.23921 -2.06422
C 3.36991 -4.06589 -1.42213
H 3.82009 -4.94049 -0.94718
C 1.98360 -3.89836 -1.38711
H 1.34204 -4.62349 -0.88337
C 1.41654 -2.77076 -1.98680
C -1.41635 -2.77103 1.98645
C -2.21318 -1.81155 2.61576
H -1.74710 -0.93765 3.07213
C -3.59789 -1.98591 2.64293
H -4.22626 -1.23657 3.12830
C -4.17719 -3.11054 2.04661
H -5.26174 -3.23962 2.06386
C -3.36969 -4.06617 1.42166
H -3.81984 -4.94073 0.94662
C -1.98338 -3.89859 1.38664
H -1.34179 -4.62365 0.88282
C 0.95061 -3.48631 2.40229
H 0.66578 -4.38680 2.93934
C 2.17008 -2.98556 2.07950
H 3.17159 -3.36441 2.26047
C 0.57634 -1.53046 1.29246
C 2.85583 -0.94893 0.75668
C 4.24779 -1.00662 0.82872
H 4.76388 -1.75216 1.43232

C 4.94943 -0.04875 0.08472
H 6.04106 -0.05527 0.10754
C 4.29100 0.91829 -0.68590
H 4.84043 1.66077 -1.26315
C 2.89644 0.87731 -0.67215
C 0.64569 1.51257 -1.26153
C 2.28970 2.93342 -2.00543
H 3.30332 3.29052 -2.16163
C 1.08993 3.46371 -2.35324
H 0.83933 4.37264 -2.89309
C -1.84804 3.97328 -1.46139
H -1.19606 4.70867 -0.98683
C -3.22917 4.17339 -1.52618
H -3.66260 5.08326 -1.10495
C -4.05282 3.20699 -2.11221
H -5.13325 3.36263 -2.15348
C -3.49409 2.03872 -2.64074
H -4.13443 1.28126 -3.09687
C -2.11513 1.83097 -2.58333
H -1.66570 0.92405 -2.98863
C -1.30169 2.80164 -1.99257

$[Mn(bim^{Ph})_2]^{2+}$ (S = 5/2)

Energy = -3470.37007537
Enthalpy 0K = -3469.657558
Enthalpy 298K = -3469.612036
Free Energy 298K = -3469.739446
Nimag = 0 (12.5621 cm^{-1})

Mn -0.00672 0.00014 -0.00017
N 2.86290 0.31428 1.78951
N 1.97089 2.19270 1.28982
N 0.04596 2.48246 0.09026
N -1.87882 2.35389 -1.13657
N -2.86244 0.54993 -1.73032
N -2.86306 -0.53144 1.73148
N -1.89306 -2.34186 1.13458
N 0.03119 -2.48242 -0.09197
N 1.95857 -2.20519 -1.29066
N 2.86492 -0.33305 -1.78769
C 3.08014 -1.09332 1.89223
C 2.06718 -1.91281 2.40069
H 1.13830 -1.46630 2.75466
C 2.26050 -3.29392 2.44602
H 1.46662 -3.93607 2.83311

C 3.46101 -3.85288 1.99612
H 3.60688 -4.93490 2.02869
C 4.47301 -3.02398 1.50236
H 5.40989 -3.45507 1.14249
C 4.28589 -1.64091 1.44383
H 5.05963 -0.99228 1.03021
C 3.79313 1.29933 2.12942
H 4.75823 1.06347 2.56906
C 3.22479 2.49175 1.81716
H 3.60559 3.50400 1.91134
C 1.73165 0.84425 1.27209
C 1.03923 3.09206 0.71662
C 1.14114 4.48363 0.77140
H 1.95455 4.98251 1.29607
C 0.14468 5.21356 0.11556
H 0.18460 6.30459 0.12536
C -0.89927 4.56991 -0.55714
H -1.67085 5.13491 -1.07863
C -0.89676 3.17409 -0.52938
C -1.70590 0.99730 -1.19070
C -3.11762 2.74083 -1.64201
H -3.44957 3.77369 -1.67770
C -3.74401 1.59531 -2.01413
H -4.72149 1.42990 -2.45842
C -2.17644 -1.68894 -2.42639
H -1.22368 -1.27746 -2.75847
C -2.43888 -3.05626 -2.52257
H -1.67606 -3.72368 -2.92918
C -3.67083 -3.56956 -2.10407
H -3.87118 -4.64080 -2.17867
C -4.64475 -2.70844 -1.58935
H -5.60604 -3.10376 -1.25356
C -4.38742 -1.34028 -1.47616
H -5.12977 -0.66847 -1.04248
C -3.15086 -0.83861 -1.89417
C -3.14140 0.85913 1.89617
C -2.15908 1.70273 2.42457
H -1.20801 1.28470 2.75326
C -2.41145 3.07190 2.52118
H -1.64238 3.73401 2.92470
C -3.64120 3.59382 2.10691
H -3.83366 4.66648 2.18182
C -4.62304 2.73946 1.59593
H -5.58266 3.14152 1.26340
C -4.37584 1.36947 1.48234
H -5.12442 0.70286 1.05130

C -3.75068 -1.57105 2.01765
H -4.72567 -1.39930 2.46499
C -3.13297 -2.72063 1.64352
H -3.47171 -3.75123 1.68034
C -1.71105 -0.98651 1.18868
C -0.91757 -3.16819 0.52507
C -0.93187 -4.56402 0.54813
H -1.70846 -5.12435 1.06727
C 0.10681 -5.21423 -0.12641
H 0.13735 -6.30554 -0.13999
C 1.10947 -4.49055 -0.77969
H 1.91856 -4.99442 -1.30632
C 1.01929 -3.09835 -0.72030
C 1.72836 -0.85514 -1.27394
C 3.21225 -2.51287 -1.81356
H 3.58670 -3.52768 -1.90566
C 3.78966 -1.32442 -2.12423
H 4.75787 -1.09511 -2.56048
C 4.29960 1.61268 -1.43750
H 5.06738 0.95903 -1.02069
C 4.49630 2.99441 -1.49611
H 5.43478 3.41935 -1.13307
C 3.49176 3.82981 -1.99411
H 3.64507 4.91080 -2.02677
C 2.28911 3.27872 -2.44805
H 1.50107 3.92602 -2.83846
C 2.08628 1.89897 -2.40267
H 1.15575 1.45848 -2.75985
C 3.09190 1.07299 -1.89013

References

1 E. Peris, J. Mata, J. A. Loch and R. H. Crabtree, *Chem. Commun.*, 2001, 201–202.
2 Y. Vukadinovic, L. Burkhardt, A. Päpcke, A. Miletic, L. Fritsch, B. Altenburger, R. Schoch, A. Neuba, S. Lochbrunner and M. Bauer, *Inorg. Chem.*, 2020, **59**, 8762–8774.
3 CrysAlisPro 1.171.43.120a Rikagu OD 2024.
4 R. C. Clark and J. S. Reid, *Acta Crystallogr A Found Crystallogr*, 1995, **51**, 887–897.
5 G. M. Sheldrick, *Acta Crystallographica*, 2015, **A71**, 3–8.
6 G. M. Sheldrick, *Acta Crystallographica*, 2015, **C71**, 3–8.
7 O. V. Dolomanov, L. J. Bourhis, R. J. Gildea, J. A. K. Howard and H. Puschmann, *Journal of Applied Crystallography*, 2009, **42**, 339–341.
8 A. M. Brouwer, *Pure and Applied Chemistry*, 2011, **83**, 2213–2228.
9 D. M. Arias-Rotondo and J. K. McCusker, *Chem. Soc. Rev.*, 2016, **45**, 5803–5820.
10 H. A. Pillman and G. J. Blanchard, *J. Phys. Chem. B*, 2010, **114**, 3840–3846.
11 M. J. Frisch, G. W. Trucks, H. B. Schlegel, G. E. Scuseria, M. A. Robb, J. R. Cheeseman, G. Scalmani, V. Barone, G. A. Petersson, H. Nakatsuji, X. Li, M. Caricato, A. V. Marenich, J. Bloino, B. G. Janesko, R. Gomperts, B. Mennucci, H. P. Hratchian, J. V. Ortiz, A. F. Izmaylov, J. L. Sonnenberg, Williams, F. Ding, F. Lipparini, F. Egidi, J. Goings, B. Peng, A. Petrone, T. Henderson, D. Ranasinghe, V. G. Zakrzewski, J. Gao, N. Rega, G. Zheng, W. Liang, M. Hada, M. Ehara, K. Toyota, R. Fukuda, J. Hasegawa, M. Ishida, T. Nakajima, Y. Honda, O. Kitao, H. Nakai, T. Vreven, K. Throssell, J. A. Montgomery Jr., J. E. Peralta, F. Ogliaro, M. J. Bearpark, J. J. Heyd, E. N. Brothers, K. N. Kudin, V. N. Staroverov, T. A. Keith, R. Kobayashi, J. Normand, K. Raghavachari, A. P. Rendell, J. C. Burant, S. S. Iyengar, J. Tomasi, M. Cossi, J. M. Millam, M. Klene, C. Adamo, R. Cammi, J. W. Ochterski, R. L. Martin, K. Morokuma, O. Farkas, J. B. Foresman and D. J. Fox, Gaussian 16 Rev. A.03 2016.
12 A. D. Becke, *J. Chem. Phys.*, 1993, **98**, 5648–5652.
13 S. Grimme, S. Ehrlich and L. Goerigk, *J Comput Chem*, 2011, **32**, 1456–1465.
14 A. V. Marenich, C. J. Cramer and D. G. Truhlar, *J. Phys. Chem. B*, 2009, **113**, 6378–6396.
15 F. Weigend and R. Ahlrichs, *Phys. Chem. Chem. Phys.*, 2005, **7**, 3297.
16 F. Weigend, *Phys. Chem. Chem. Phys.*, 2006, **8**, 1057.
17 S. Grimme, *Chem. - Eur. J.*, 2012, **18**, 9955–9964.
18 S. T. Sahil, K. M. McCardle, P. Le Magueres, J. A. Panetier and J. W. Jurss, *ACS Omega*, 2024, **9**, 34555–34566.
19 R. K. Wilson and S. Brooker, *Dalton Trans.*, 2013, **42**, 12075.
20 S. Heider, H. Petzold and G. Teucher, *Eur J Inorg Chem*, 2013, **2013**, 2382–2388.
21 S. De, S. Tewary, D. Garnier, Y. Li, G. Gontard, L. Lisnard, A. Flambard, F. Breher, M. Boillot, G. Rajaraman and R. Lescouëzec, *Eur J Inorg Chem*, 2018, **2018**, 414–428.
22 T. H. Crawford and J. Swanson, *J. Chem. Educ.*, 1971, **48**, 382.
23 G. A. Bain and J. F. Berry, *J. Chem. Educ.*, 2008, **85**, 532.
24 D. Pugh, J. A. Wright, S. Freeman and A. A. Danopoulos, *Dalton Trans.*, 2006, 775–782.